Nanoscale

PAPER

View Article Online
View Journal

Check for updates

Cite this: DOI: 10.1039/c9nr03707a

# Hybrid light emitting diodes based on stable, high brightness all-inorganic $CsPbI_3$ perovskite nanocrystals and InGaN†

Chengxi Zhang, *[a,b] Lyudmila Turyanska, *[a,c] Haicheng Cao, [d] Lixia Zhao, [d] Michael W. Fay, [e] Robert Temperton, [a] James O'Shea,[a] Neil R. Thomas, [f] Kaiyou Wang, [g] Weiling Luan[b] and Amalia Patanè*[a]

Received 30th April 2019,
Accepted 4th June 2019

DOI: 10.1039/c9nr03707a

rsc.li/nanoscale

Despite important advances in the synthesis of inorganic perovskite nanocrystals (NCs), the long-term instability and degradation of their quantum yield (QY) over time need to be addressed to enable the further development and exploitation of these nanomaterials. Here we report stable $CsPbI_3$ perovskite NCs and their use in hybrid light emitting diodes (LEDs), which combine in one system the NCs and a blue GaN-based LED. Nanocrystals with improved morphological and optical properties are obtained by optimizing the post-synthesis replacement of oleic acid ligands with iminodibenzoic acid: the NCs have a long shelf-life (>2 months), stability under different environmental conditions, and a high QY, of up to 90%, in the visible spectral range. Ligand replacement enables the engineering of the morphological and optical properties of the NCs. Furthermore, the NCs can be used to coat the surface of a GaN-LED to realize a stable diode where they are excited by blue light from the LED under low current injection conditions, resulting in emissions at distinct wavelengths in the visible range. The high QY and fluorescence lifetime in the nanosecond range are key parameters for visible light communication, an emerging technology that requires high-performance visible light sources for secure, fast energy-efficient wireless transmission.

Open Access Article. Published on 09 July 2019. Downloaded on 7/10/2019 9:06:30 AM.
This article is licensed under a Creative Commons Attribution 3.0 Unported Licence.

## 1. Introduction

The development of colloidal halide perovskite nanocrystals (NCs) has attracted global attention since their first synthesis in 2015.[1] Of particular interest are all-inorganic cesium lead halide perovskite NCs ($CsPbX_3$, X = Cl, Br, and I or mixed). They have a band gap energy tunable in a wide spectral range, narrow emission lines and high photoluminescence (PL) quantum yield (QY).[1–3] These nanomaterials have potential applications in optoelectronics,[4–13] including lasers,[5] solar cells,[6,7] screen displays,[8] light-emitting diodes (LEDs)[9–11,14,15] and photodetectors.[12,16] However, despite recent important advances in their synthesis and exploitation,[10,12,13,16,17] the long-term instability and degradation of the QY over time should be addressed to enable the emergence of a robust class of materials for fundamental and applied research. Furthermore, the chemical decomposition of the NCs due to their exposure to specific environments, such as air, light, and/or high temperatures, can result in the release of toxic ions to the environment, representing a drawback to their sustainable use.

The stability of $CsPbX_3$ NCs is affected by the strength of binding, surface density and stability of the capping molecules. Oleic acid (OA), oleylamine (OLA), and trioctylphosphine oxide (TOPO) are commonly used as capping ligands,[17] but fail to prevent the degradation of the NCs over time. On the other hand, bidentate ligands, such as iminodibenzoic acid (IDA) and didodecyldimethylammonium bromide (DDAB), can improve the NC stability due to their coordination to two sites on the NC surface and a stronger steric effect.[18,19] However, the effects of replacement conditions on the stability and properties of the NCs remain unexplored. The strength of attachment of capping ligands is of paramount importance for stabilization of the chemical composition of the NCs in different environments, thus reducing their toxicity. In particular, a significant fraction (>10%) of the atoms of the NC lie on the surface. These may have unsaturated bonds that act as non-radiative recombination centres for charge carriers, thus reducing the QY. The presence

[a]School of Physics and Astronomy, University of Nottingham, NG7 2RD, UK. E-mail: lyudmila.turyanska@nottingham.ac.uk, amalia.patane@nottingham.ac.uk, xi1273424183@163.com
[b]East China University of Science and Technology, Shanghai 200237, China
[c]School of Chemistry, University of Lincoln, Lincoln LN6 7TS, UK
[d]Institute of Semiconductors, Chinese Academy of Sciences, Beijing 100083, China
[e]Nanoscale and Microscale Research Centre, University of Nottingham, NG7 2RD, UK
[f]Centre for Biomolecular Sciences, School of Chemistry, University of Nottingham, University Park, NG7 2RD, UK
[g]State Key Laboratory of Superlattices and Microstructures, Institute of Semiconductors, Chinese Academy of Sciences, Beijing 100083, China

†Electronic supplementary information (ESI) available. See DOI: 10.1039/c9nr03707a

Open Access Article. Published on 09 July 2019. Downloaded on 7/10/2019 9:06:30 AM.
This article is licensed under a Creative Commons Attribution 3.0 Unported Licence.

of amino- and carboxylic-functional groups in the capping molecules can enable the coordination to and passivation of $Pb^{2+}$ and $Br^-$ surface defects.[20–22] Hence, solution phase ligand exchange can provide a tool for modifying the NC surface and improving the QY.[23–25] The controlled modification of the NC surface can also offer a route to engineering the interface of the NCs with other material systems to facilitate and/or inhibit charge transfer for specific applications.[26] In summary, despite the emergence of new surface passivation approaches, there is still a need for strategies to produce stable perovskite NCs and tailor their surface in a controlled fashion.

Here, we report on the investigation of the post-synthesis surface passivation of $CsPbI_3$ NCs by ligand replacement and the use of the NCs in solid state light emitting diodes (LEDs). We use bidentate 2,2′-iminodibenzoic acid (IDA) ligands to replace oleic acid (Fig. 1a) and examine the effect of replacement conditions (quantity of the ligands and replacement temperature) on the stability and QY of the NCs. Optimization of the conditions for ligand replacement enables us to achieve a significant increase of the NC shelf life and QY, and stability of the NCs under different environmental conditions. We demonstrate the successful implementation of these NCs in a novel type of hybrid light emitting device (Fig. 1b), where the NCs coat the surface of a GaN-based LED. The NCs are excited by blue-light from the LED to emit in the VIS spectral range under low current injection conditions. The combination of the perovskite NCs with an established III–V semiconductor technology offers opportunities for further important developments. In particular, the high QY and short fluorescence lifetime of the NCs are directly relevant to visible light communication (VLC), an emerging technology that requires high-performance visible light sources for secure, fast and energy-efficient wireless transmission.[27]

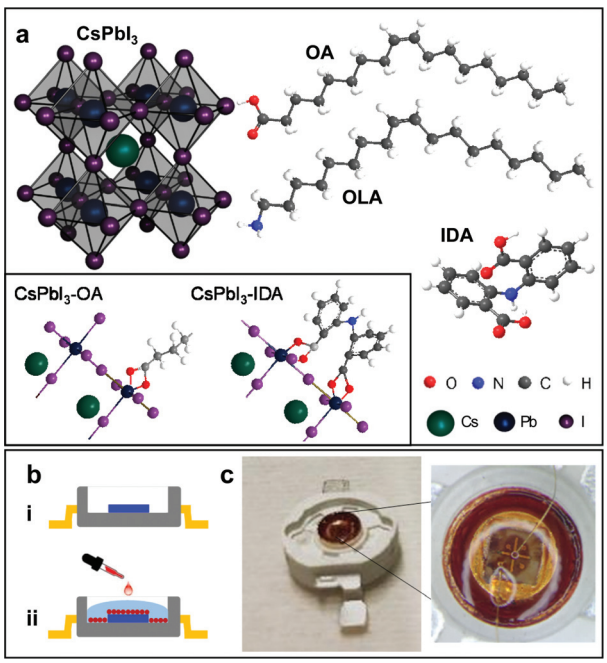



Fig. 1 (a) Schematic of a $CsPbI_3$ nanocrystal (NC) and of oleic acid (OA), oleylamine (OLA) and bidentate 2,2′-iminodibenzoic acid (IDA) ligands. The left inset illustrates the coordination of OA and IDA to the $Pb^{2+}$ ions on the NC surface: the single carboxylic group of OA binds to 1 $Pb^{2+}$ ion; the double carboxylic groups of IDA bind to 2 $Pb^{2+}$ ions. (b) Two-step fabrication of a light emitting device based on $CsPbI_3$ NCs: (i) fabrication of a GaN-based LED followed by (ii) coating of the LED surface with $CsPbI_3$ NCs and encapsulation with a protective layer of methyl silicone rubber. (c) Optical images of a light emitting device based on GaN and NCs on a chip carrier.

## 2. Results and discussion

### 2.1 $CsPbI_3$ nanocrystals: enhanced shell-life and quantum yield by ligand replacement

$CsPbI_3$ perovskite nanocrystals were synthesized following and further developing a method from Chen *et al.*[28] to replace OA with IDA (see Experimental section). Our strategy is based on the controlled modification of the nanocrystal surface by IDA to optimize the coordination to and passivation of surface defects, and stability under different environmental conditions. For ligand replacement, IDA was added to the NC solution at different concentrations and ligand replacement was performed at different temperatures $T_{IDA}$ from room temperature to 80 °C. After purification, the NCs were dispersed in *n*-hexane and stored under nitrogen atmosphere at $T$ = 5 °C, and examined periodically over at least 2 months.

The energy-dispersive X-ray (EDX) and X-ray photoelectron spectroscopy (XPS) studies on control (*i.e.* no IDA) and IDA-treated NCs reveal the elements and stoichiometry expected for $CsPbI_3$ (ESI SI1†). The high-resolution XPS spectra show the N 1s peak due to the OLA and/or IDA ligands. From the integrated area of the XPS lines at the energy of Pb 4f and N 1s, we estimate that the atomic ratio of N : Pb increases in the IDA-based samples. The IDA-ligand replacement is further supported by NMR studies, revealing characteristic spectral signatures in the aromatic range (ESI, SI1†).

Optical spectroscopy experiments were conducted on NCs drop-cast on a transparent quartz substrate in air (PL) or on NC solutions (PL, absorption, and QY studies). As shown in Fig. 2, for freshly synthesized control (*i.e.* no IDA) solutions, the PL peak is centred at $\lambda$ = 670 nm and has a QY of 75%. Following the treatment with IDA ($Pb^{2+}$ : IDA = 5 : 1 and $T_{IDA}$ = 40 °C), the PL peak shifts to $\lambda$ = 680 nm and the QY increases to 85%. Thus, freshly prepared solutions of NCs with and without IDA exhibit similar PL properties. However, the IDA ligand exchange leads to a significant improvement of the NC shelf life: for the control sample, no PL signal is observed after 25 days of storage; in contrast, no degradation is observed for treated with IDA, which also show a stronger absorption (Fig. 2). These data demonstrate a more efficient stabilization of the NCs by IDA, which provide two binding sites to the NC surface (inset in Fig. 1a), hence enhancing the NC passivation. The coordination of this type of ligands to the surface of a nanocrystal was previously reported for metal nanoparticles and semiconductor quantum dots, including perovskite

 This journal is © The Royal Society of Chemistry 2019

Open Access Article. Published on 09 July 2019. Downloaded on 7/10/2019 9:06:30 AM.
This article is licensed under a Creative Commons Attribution 3.0 Unported Licence.

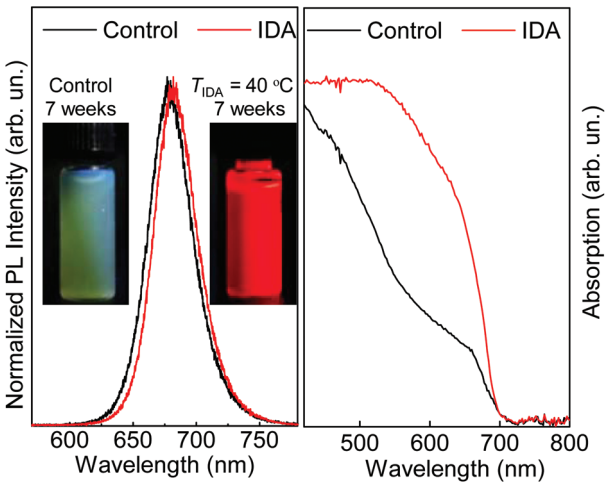



**Fig. 2** Room temperature normalized photoluminescence (left) and absorption (right) spectra of 2 weeks old nanocrystal solutions with and without IDA. The insets show photographs of the solutions under UV light, 7 weeks after synthesis.

nanocrystals.[10,29,30] Hence, we examine further the NC passivation by IDA using different replacement conditions.

We have examined NC solutions with different concentration of IDA and observed the largest QY for $Pb^{2+}$ : IDA = 5 : 1 (ESI SI2†). Guided by these results, samples with a molar ratio of $Pb^{2+}$ : IDA = 5 : 1 were used to investigate the efficiency of the IDA replacement at various temperatures $T_{IDA}$ (Fig. 3a and b). For $T_{IDA}$ = 23 °C, the QY has a value of up to 75%, comparable to that reported in the literature,[10] but decreases to less than 30% after a period of 30 days. Samples treated with IDA at higher temperature ($T_{IDA}$ = 40, 60 and 80 °C) show a different behaviour: the QY increases by up to 92% and is stable for up to 30 days (Fig. 3a and b), indicating a greater stability of the capping layer and improved passivation of the NC surface by IDA.

The improved shelf-life of the NCs is accompanied by an increased resilience of the nanocrystals to photodegradation. The degradation of the QY is time- and light wavelength-dependent, and is stronger under UV light excitation in air (inset of Fig. 3a) and/or at high temperatures ($T$ > 100 °C). The reduced QY is not accompanied by any change of the PL peak energy. However, exposure of the NCs to air at high temperatures ($T$ > 100 °C) tends to decrease the lifetime $\tau$ from tens to just a few nanoseconds (2–3 ns). This decrease of $\tau$ indicates an increased density of non-radiative recombination centres on the surface of the nanocrystals (ESI SI3†). In general, the IDA ligands provide improved stabilization of the nanocrystals against different environmental components. Thus, the degradation is likely to occur on the surface of the NCs and may involve photo-oxidative and/or thermo-oxidative reactions.[31–33]

### 2.2 Effect of ligand replacement on the morphology of $CsPbI_3$ nanocrystals

For the transmission electron microscopy (TEM) and high resolution TEM (HRTEM) studies, the NC solutions were drop-cast on graphene oxide coated copper grids. The TEM images

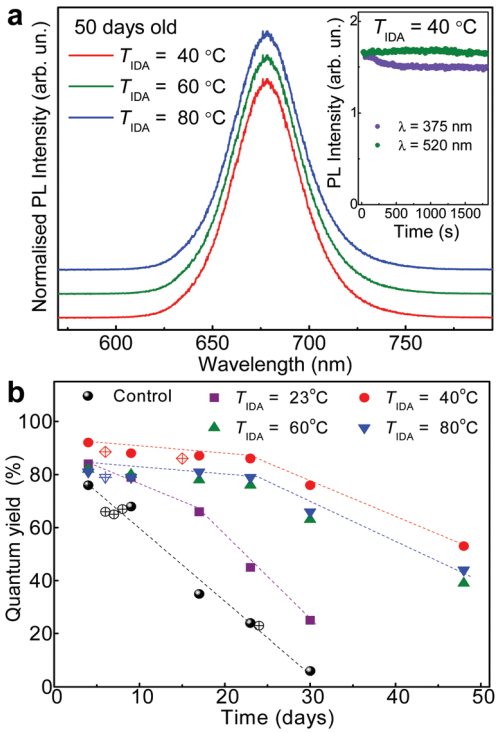



**Fig. 3** (a) Normalized photoluminescence (PL) spectra of IDA-treated $CsPbI_3$ nanocrystals 50 days after synthesis ($T_{IDA}$ = 23, 40, 60 and 80 °C). The inset shows the temporal evolution of the PL peak intensity for IDA-capped $CsPbI_3$ nanocrystals ($T_{IDA}$ = 40 °C) under excitation with light of wavelength $\lambda$ = 520 and 370 nm. (b) PL QY of control and IDA-treated $CsPbI_3$ nanocrystals at different times after synthesis.

show that OA/OLA capped NCs are cubic particles with an average size $d_{NC}$ = 21.3 ± 3.3 nm, as probed soon after the synthesis of the NCs (Fig. 4 and ESI SI4†). This value tends to decrease to $d_{NC}$ = 16.6 ± 2.8 nm following 20-day storage of the solution. From the HRTEM images, we estimate interplanar distances of 4.26 Å and 6.04 Å corresponding to the (110) and (100) crystal planes of cubic $CsPbI_3$.[2,10] Ligand exchange with IDA at room temperature ($T_{IDA}$ = 23 °C) does not affect significantly the size of the NCs. However, for $T_{IDA}$ in the range 40 °C to 80 °C, the nanocrystals have a smaller average size and narrower size distribution (Fig. 4b–d): the average size is $d_{NC}$ = 12.9 ± 1.7 nm at $T_{IDA}$ = 40 °C and decreases to $d_{NC}$ = 9.3 ± 1.5 nm at $T_{IDA}$ = 80 °C. Also, no significant change of the NC average size or shape was observed over a period of at least 20 days.

The IDA-treated NCs have the same crystal lattice parameters as the control sample, indicating that their crystal structure and composition are not altered by the ligand exchange and/or treatment temperature. On the other hand, the average size and size distribution of the nanocrystals are modified. The narrowing of the NC size distribution and its stability for $T_{IDA} \geq$ 40 °C are accompanied by an increase in the shelf-life, QY and absorption of the NCs (Fig. 2 and 3). Despite the change in the average size of the NCs, the PL peak energy does not change, indicating that the spectral properties of the NCs are primarily determined by the composition rather

Open Access Article. Published on 09 July 2019. Downloaded on 7/10/2019 9:06:30 AM.
This article is licensed under a Creative Commons Attribution 3.0 Unported Licence.

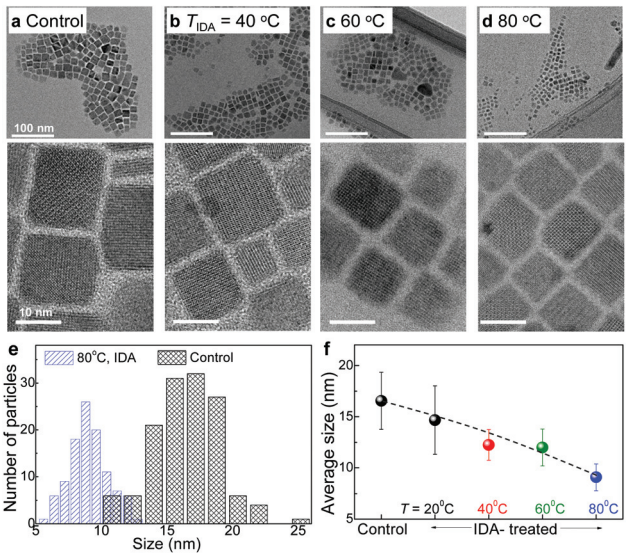



**Fig. 4** (a) Transmission electron microscopy (TEM) and high resolution TEM (HRTEM) images of a control sample and $CsPbI_3$ nanocrystals (NCs) treated with IDA at (b) $T_{IDA}$ = 40 °C, (c) $T_{IDA}$ = 60 °C, and (d) $T_{IDA}$ = 80 °C. (e) NC size distribution for the control and IDA-treated nanocrystals ($T_{IDA}$ = 80 °C). (f) Average size of the NCs for different samples.

than the NC size.[34] Also, the PL intensity and QY improve, indicating a more effective passivation of surface defects by IDA, as reported for nanocrystals capped with a high density of surface ligands.[35]

The IDA ligands with their bidentate carboxylic groups can coordinate to two separate $Pb^{2+}$-ions, providing greater NC stability compared to OA that coordinates to a single $Pb^{2+}$ with a lower binding energy (Fig. 1a).[10] Thus the IDA ligands enable a more effective passivation of surface defects.[18] For temperatures $T_{IDA} \geq 40$ °C, a larger concentration of OA is replaced by IDA, as observed in XPS (ESI SI1†). The interaction between the ligands and surface atoms on the NCs is a dynamic process: as OA is replaced by IDA, surface atoms on the OA tend to leave the NC, thus resulting in smaller nanoparticles. Thus, ligand exchange at specific temperatures can promote the formation of smaller, more uniform and stable NCs, as shown by TEM (Fig. 4).

The surface passivation of perovskite NCs is essential to retain the stability of their cubic phase;[36] also, post-synthesis thermal treatments can promote a more uniform distribution of Pb throughout the nanocrystal.[37] We envisage that both phenomena contribute to an increase of QY. In our IDA-treated NCs, the QY is increased by up to ~90% and retained over a period of at least 30 days. The high QY is comparable to that achieved with significantly more toxic and less stable trioctylphosphine oxide (TOPO)[2] and thiocyanate capping ligands.[38] We note that our approach allows to preserve the crystal structure of the nanocrystals following ligand exchange. Also, the improved stability is not related to the morphological changes observed in lead halide-ligand treated perovskites,[39,40] but is governed by strong binding of bidentate ligands to the NC surface. Thus, our approach provides a simple, reproducible up-scalable route for the synthesis of high-brightness and stable NCs, suitable for integration into functional devices, as discussed below.

### 2.3 Light emitting devices based on GaN-LEDs and $CsPbI_3$ nanocrystals

Our light emitting devices combine in one structure the IDA-based $CsPbI_3$ perovskite NCs and blue GaN-based LEDs. Fig. 1b–c sketches the fabrication process and the optical images of a representative device on a chip carrier. For the GaN-based LED, a p–n junction with an InGaN/GaN multi-quantum well (MQW) optically active region was first grown on a 2-inch diameter (0001)-orientation (*c*-plane) sapphire substrate by using metal organic chemical vapour deposition (MOCVD). The wafer was processed into LED chips of diameter $d$ = 120 μm by using standard microfabrication techniques[41] (see Experimental section). Following the LED fabrication, a solution of the NCs in hexane (concentration 15 mg $mL^{-1}$, $T_{IDA}$ = 40 °C) was dropped cast on the surface of the LED using a syringe. The solvent (hexane) on the LED surface was evaporated under pumping inside a vacuum chamber. After repeated drop casting and solvent evaporation steps to increase the concentration of the NCs, the LED was coated with a protective layer of methyl silicone rubber (KER 2500, Shin-Etsu), which possesses high optical transparency, low refractive index ($n$ = 1.4), chemical inertness, and high-temperature stability.[42,43] This coating is commonly used in commercial LEDs to improve light extraction and avoid contamination and degradation of the diodes in air.

Fig. 5a shows the room temperature ($T$ = 300 K) electroluminescence (EL) spectra for one of our devices under injection currents $I$ = 10, 20 and 40 mA. The EL emission from the InGaN/GaN MQW is peaked at a wavelength $\lambda$ = 475 nm. The EL spectra also clearly reveal the optical emission from the NCs at $\lambda$ = 690 nm, matching the PL peak emission wavelength of the NC solutions (Fig. 2). Thus, the NCs can be effectively excited under relatively low injection current conditions with the intensity of the NC optical emission being comparable to that of the InGaN/GaN MQW. The EL intensity from the InGaN/GaN MQW increases with increasing $I$ and tends to saturate at $I$ > 20 mA, corresponding to optical powers $P$ > 50 W $cm^{-2}$. This saturation behaviour is accompanied by a corresponding saturation of the optical emission of the NCs, which we assign to the relatively low density of states of the NCs in the film. We have examined the stability of the LED under electrical pumping: after about 5 minutes of operation at a constant current ($I$ = 10 mA), the NC emission intensity reaches a stable value, which is maintained over a period of at least 1 hour (Fig. 5b).

The QY and fluorescence lifetime of the NCs are crucial parameters for exploitation in visible light communication. Commercial lighting and communication systems make use of blue GaN-based LEDs and cerium-doped phosphors converting blue light into green, yellow, and/or red emission. However, the overall bandwidth of such devices is of a few MHz due to the long fluorescence lifetime of conventional


This journal is © The Royal Society of Chemistry 2019

Open Access Article. Published on 09 July 2019. Downloaded on 7/10/2019 9:06:30 AM.
This article is licensed under a Creative Commons Attribution 3.0 Unported Licence.

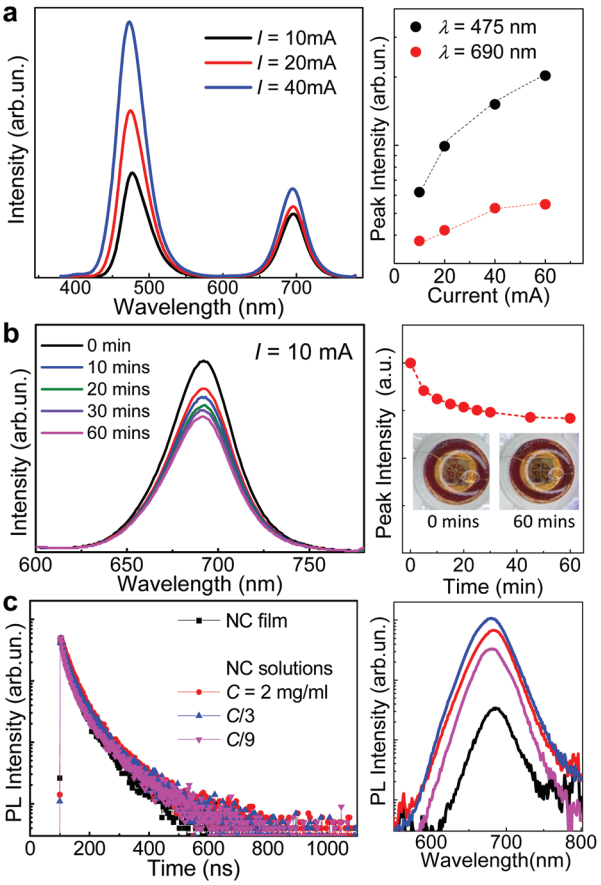



**Fig. 5** (a) Left: Room temperature ($T$ = 300 K) luminescence spectra for an hybrid-LED under different injection currents $I$ = 10, 20, 40 mA. Right: $I$-Dependence of the luminescence intensity for the InGaN/GaN MQW ($\lambda$ = 475 nm) and nanocrystals ($\lambda$ = 690 nm). (b) Left: Room temperature ($T$ = 300 K) luminescence spectra for the nanocrystals at different times under continuous operation ($I$ = 10 mA). Right: Time-dependence of the peak intensity ($\lambda$ = 690 nm). Insets: Images of the LED at the start and end of the measurement. (c) Left: Time-decay of the photoluminescence (PL) intensity at $\lambda$ = 690 nm for a film and solutions of nanocrystals with different concentrations ($T$ = 300 K). Right: Typical PL spectra of the NC film and solutions.

phosphors,[44] thus representing a drawback for exploitation in high-speed communication systems. In contrast, perovskite NCs generally have fluorescent lifetimes of the order of a few or tens of nanoseconds.[2,6,45] In particular, $CsPbBr_3$ NCs have shown potential as fast colour converters for VLC: they have a modulation bandwidth of 491 MHz,[46] significantly larger than that of conventional phosphors.

Fig. 5c shows the time-resolved PL (TRPL) decay curves and corresponding PL spectra for 4 samples based on thin NC films and solutions of IDA-based $CsPbI_3$ NCs with different concentrations. All samples exhibit similar PL spectra. Thus, the TRPL experiments were performed by detecting the PL intensity at the peak energy of the PL band. The fluorescence decay traces reveal a similar behaviour with a fast decay component and lifetimes (25–30 ns) comparable to those reported for $CsPbI_3$ NCs with OA/OLA ($\tau$ = 22 ns) or TOPO ($\tau$ = 36 ns)

**Table 1** Fluorescence lifetimes for films and solutions of IDA-treated $CsPbI_3$ perovskite NCs. Data in the table are derived from fits to the measured TRPL curves with two exponential-decay functions. Here $\tau_i$ is the lifetime of one decay component and $A_i$ its fractional amplitude; $\chi^2$ is the reduced chi-squared statistic and $\tau$ is an average lifetime given by = $(A_1\tau_1^2 + A_2\tau_2^2)/(A_1\tau_1 + A_2\tau_2)$

| | | NC solutions | | |
|---|---|---|---|---|
| | NC film | $C$ = 2 mg mL$^{-1}$ | $C$/3 | $C$/9 |
| $\tau_1$ (ns) | 27 | 30 | 26 | 25 |
| $A_1$ | 64% | 74% | 65% | 58% |
| $\tau_2$ (ns) | 114 | 112 | 98 | 113 |
| $A_2$ | 36% | 26% | 35% | 42% |
| $\chi^2$ | 1.2 | 1.0 | 1.0 | 1.3 |
| $\tau$ (ns) | 88 | 77 | 74 | 92 |

ligands.[2] An additional weaker slow (~100 ns) decay component is also observed. Dual or multiple lifetimes are suggestive of different relaxation pathways for the charge carriers due to charged states and/or traps in and/or outside the nanocrystals, and/or different local environments.[47] In particular, the contribution of a weak slow decay can arise from screening effects by inorganic ligands or interaction of carriers with acoustic and optical phonons.[48,49] Table 1 shows the lifetimes, $\tau_1$ and $\tau_2$, extracted from the fit of the TRPL decay curves by the sum of two exponential decay functions and the corresponding average lifetime. Our data show that the density of the NCs and their environment (*e.g.* solvent or air) do not have a significant effect on the value of $\tau$ at room temperature.

In summary, we have demonstrated the successful fabrication of a compact hybrid LED structure based on IDA-based $CsPbI_3$ perovskite NCs. The high QY (up to 90%), improved environmental stability and short fluorescent lifetime of the NCs can provide a promising platform for the development of a new class of visible emitters that combine in one structure different materials and that can be operated reproducibly under low current injection conditions.

## 3. Conclusions

In conclusion, we have demonstrated a reliable approach to the synthesis of high-brightness, stable $CsPbI_3$ perovskite nanocrystals. The use of bidentate 2,2′-iminodibenzoic acid (IDA) ligands to replace oleic acid (OA) and oleylamine (OLA) ligands provides an effective way of passivating the surface of the nanocrystals, resulting in nanocrystals with a smaller average size, a significant increase in their shelf-life and quantum yield, and improved stability under different environmental conditions. The high-quality of the nanocrystals enables the successful fabrication of light emitting devices where the nanocrystals are integrated on the surface of a GaN-based LED. They are excited by blue light to emit in the visible spectral range under low current injection conditions. The fluorescence lifetime of the nanocrystals is in the nanosecond range and could be further decreased by post-synthesis treat-

Open Access Article. Published on 09 July 2019. Downloaded on 7/10/2019 9:06:30 AM.
This article is licensed under a Creative Commons Attribution 3.0 Unported Licence.

ment of the nanocrystals through the controlled incorporation of dopants acting as radiative recombination centres, which requires further investigation. The hybrid LED demonstrated here, combining colloidal nanocrystals with a well-established III–V semiconductor LED, is of particular interest as it opens up interesting avenues for integration of novel colloidal materials with emerging technologies. For example, we envisage the implementation of our approach to lead-free perovskite (*e.g.* $CsSnI_3$, $CsSnBr_3$), and nanocrystals with different compositions (*e.g.* $CuInS_2$) to tune the spectral response of the nanocrystals, as required to optimize their use in different optical components[26] and VLC systems.

# 4. Experimental section

## 4.1 Materials and synthesis

Lead(II) iodide ($PbI_2$, 99.999%), cesium carbonate ($Cs_2CO_3$, 99.95%), oleic acid (OA, 90%), oleylamine (OLA, 70%), 1-octadecene (ODE, 90%), ethyl acetate (EA, anhydrous, 99.8%), hexane (anhydrous, 95%) and 2,2′-iminodibenzoic acid (IDA, 95%) were purchased from Sigma-Aldrich and used without further purification.

To prepare the Cs-precursor solution (Cs-oleate), 0.325 g (1 mmol) of $Cs_2CO_3$ was mixed with 9 mL ODE in a 25 mL flask and degassed at 120 °C for 10 min under nitrogen flow. Then 1.3 mL of OA was injected and the temperature increased to 150 °C. The mixture was stirred for 1 h under nitrogen flow until all the $CsCO_3$ had dissolved. The Pb-precursor solution was prepared by mixing 20 mL of ODE with 0.922 g (2 mmol) of $PbI_2$ in a 50 mL flask with stirring. The solution was degassed at 120 °C for 10 min under nitrogen flow. Then 3 mL of OA and 3 mL of OLA were injected and the mixture was stirred at 150 °C for 1 h under nitrogen flow. A clear yellow solution of $PbI_2$-OA-OLA precursor was formed.

To synthesize the $CsPbI_3$ nanocrystals, the $PbI_2$-OA-OLA precursor solution (26 mL) was heated to 160 °C and 2 mL of Cs-oleate precursor (heated to 150 °C) was quickly injected under stirring. After 20 s of mixing, the solution was cooled down on ice-bath. The solution was divided into 5 equal parts. One part was used as the reference sample and the four remaining parts were used for ligand replacement: 20 mg of IDA were added to each flask and stirred for 6 h at $T_{IDA}$ = 23 °C, 40 °C, 60 °C and 80 °C. All samples were stored under nitrogen atmosphere ($T$ = 5 °C) overnight for self-precipitation. For purification, 2.5 mL of the original solution was centrifuged at 2500 rpm for 5 min. The supernatant was further centrifuged at 12 000 rpm for 10 min. The precipitate was collected and dissolved in 3 mL of a mixture of *n*-hexane and ethylacetate (1 : 3 v/v) and centrifuged at 12 000 rpm for 10 min. Finally, the precipitate was collected and dispersed in *n*-hexane (5 mL) for storage at $T$ = 5 °C.

## 4.2 Experimental techniques

PL studies were conducted using a Horiba Jobyn Yvon micro-PL system, equipped with a frequency doubled Nd:$YVO_4$ laser ($\lambda$ = 532 nm) and Si charge-coupled device (CCD) camera. The QY was measured using an Edinburgh Instruments FLS980 fluorescence spectrometer equipped with an integrating sphere module. To obtain the QY, we compared the PL spectrum of the NCs with that of the pure solvent (hexane), used as a reference sample, under excitation with the 520 nm line of a laser diode. The QY was estimated from $\mathrm{QY} = \frac{E_{PL}^{QD} - E_{PL}^{sol}}{A_{exc}^{sol} - A_{exc}^{QD}}$, where $E_{PL}^{QD}$ ($E_{PL}^{sol}$) is the integrated intensity of the QD (solvent) PL spectrum and $A_{exc}^{QD}(A_{exc}^{sol})$ is the integrated intensity of the excitation light scattered within the integrating sphere. Time resolved photoluminescence (TRPL) spectra of the NCs were measured using a 375 nm laser diode as the excitation source with power $P$ = 2–10 μW. Electroluminescence (EL) spectra were measured using an integrating sphere in the continuous-wave mode.

Samples for energy-dispersive X-ray (EDX) and X-ray photoelectron spectroscopy (XPS) studies were prepared by drop-casting the NC solution onto a gold/mica substrate (*e.g.* XPS) or on graphene oxide coated copper grids (*e.g.* EDX). EDX studies were conducted using a JEOL-JSM-6610LV scanning electron microscope (SEM) fitted with an Oxford Instruments X-Max 800 mm energy-dispersive spectrometer. Transmission electron microscopy (TEM), high-resolution TEM (HRTEM) and selected area electron diffraction (SAED) images were acquired on a JEM-2100F, JOEL operated at 200 kV. XPS measurements were performed using a SPECS Phoibos 150 hemispherical analyser and monochromatic Al-kα (1486.7 eV) X-ray source (pressure $P = 1 \times 10^{-9}$ mbar).

## 4.3 Fabrication of LEDs

The GaN-based LED consists of a multilayer structure: 3 μm thick Si-doped GaN, four InGaN/GaN quantum wells (QWs) (thickness 3 nm/15 nm), eight pairs of Mg-doped AlGaN/GaN superlattice electron blocking layers (SL-EBL) (thickness 2 nm/2 nm), and a 62 nm thick Mg-doped GaN epilayer. Mesa areas with diameter $d$ = 120 μm were patterned by photolithography and etching. Then, Cr/Al/Ti/Au layers were deposited by electron beam evaporation to form the p-type and n-type electrodes. The electrodes were defined by lithography and lift-off techniques.

# Conflicts of interest

The authors declare no competing financial interest.

# Acknowledgements

This work was supported by the Engineering and Physical Sciences Research Council [grant numbers EP/K503800/1, NC/L001861/1]; the Defence Science and Technology Laboratory (Dstl); the University of Nottingham; the Nanoscale and Microscale Research Centre (nmRC); the National Natural Science Foundation of China under Grants 61774148 and 11574306; and the China Scholarship Council. AP acknowledges

 This journal is © The Royal Society of Chemistry 2019

Open Access Article. Published on 09 July 2019. Downloaded on 7/10/2019 9:06:30 AM.
This article is licensed under a Creative Commons Attribution 3.0 Unported Licence.

the Chinese Academy of Sciences (CAS) for the Award of a "President's International Fellowship for Visiting Scientists". The authors acknowledge useful discussions with Dr Stephen Prior.

## References

1 L. Protesescu, S. Yakunin, M. I. Bodnarchuk, F. Krieg, R. Caputo, C. H. Hendon, R. X. Yang, A. Walsh and M. V. Kovalenko, *Nano Lett.*, 2015, **15**, 3692–3696.
2 F. Liu, Y. Zhang, C. Ding, S. Kobayashi, T. Izuishi, N. Nakazawa, T. Toyoda, T. Ohta, S. Hayase, T. Minemoto, K. Yoshino, S. Dai and Q. Shen, *ACS Nano*, 2017, **11**, 10373–10383.
3 Q. Zhang and Y. Yin, *ACS Cent. Sci.*, 2018, **4**, 668–679.
4 C. C. Lin, A. Meijerink and R. S. Liu, *J. Phys. Chem. Lett.*, 2016, **7**, 495–503.
5 Y. Wang, X. M. Li, V. Nalla, H. B. Zeng and H. D. Sun, *Adv. Funct. Mater.*, 2017, **27**, 1605088.
6 B. Li, Y. N. Zhang, L. Fu, T. Yu, S. J. Zhou, L. Y. Zhang and L. W. Yin, *Nat. Commun.*, 2018, **9**, 1076.
7 D. Ghosh, M. Y. Ali, D. K. Chaudhary and S. Bhattacharyya, *Sol. Energy Mater. Sol. Cells*, 2018, **185**, 28–35.
8 D. J. Yu, F. Cao, Y. J. Gao, Y. H. Xiong and H. B. Zeng, *Adv. Funct. Mater.*, 2018, **28**, 1800248.
9 A. Subramanian, Z. H. Pan, Z. B. Zhang, I. Ahmad, J. Chen, M. N. Liu, S. Cheng, Y. J. Xu, J. Wu, W. Lei, Q. Khan and Y. G. Zhang, *ACS Appl. Mater. Interfaces*, 2018, **10**, 13236–13243.
10 J. Pan, Y. Q. Shang, J. Yin, M. De Bastiani, W. Peng, I. Dursun, L. Sinatra, A. M. El-Zohry, M. N. Hedhili, A. H. Emwas, O. F. Mohammed, Z. J. Ning and O. M. Bakr, *J. Am. Chem. Soc.*, 2018, **140**, 562–565.
11 S. Kumar, J. Jagielski, N. Kallikounis, Y. H. Kim, C. Wolf, F. Jenny, T. Tian, C. Hofer, Y.-C. Chiu, W. J. Stark, T.-W. Lee and C.-J. Shih, *Nano Lett.*, 2017, **17**, 5277–5284.
12 H. Zhou, J. P. Zeng, Z. N. Song, C. R. Grice, C. Chen, Z. H. Song, D. W. Zhao, H. Wang and Y. F. Yan, *J. Phys. Chem. Lett.*, 2018, **9**, 2043–2048.
13 Y. F. Xu, M. Z. Yang, B. X. Chen, X. D. Wang, H. Y. Chen, D. B. Kuang and C. Y. Su, *J. Am. Chem. Soc.*, 2017, **139**, 5660–5663.
14 Q. Shan, J. Song, Y. Zou, J. Li, L. Xu, J. Xue, Y. Dong, B. Han, J. Chen and H. Zeng, *Small*, 2017, **13**, 1701770.
15 J. Song, T. Fang, J. Li, L. Xu, F. Zhang, B. Han, Q. Shan and H. Zeng, *Adv. Mater.*, 2018, **30**, 1805409.
16 M. Gong, R. Sakidja, R. Goul, D. Ewing, M. Casper, A. Stramel, A. Elliot and J. Z. Wu, *ACS Nano*, 2019, **13**, 1772–1783.
17 L. Z. Wu, Q. X. Zhong, D. Yang, M. Chen, H. C. Hu, Q. Pan, H. Y. Liu, M. H. Cao, Y. Xu, B. Q. Sun and Q. Zhang, *Langmuir*, 2017, **33**, 12689–12696.
18 D. D. Yang, X. M. Li and H. B. Zeng, *Adv. Mater. Interfaces*, 2018, **5**, 1701662.
19 J. Song, J. Li, L. Xu, J. Li, F. Zhang, B. Han, Q. Shan and H. Zeng, *Adv. Mater.*, 2018, **30**, 1800764.
20 J. Kang and L. W. Wang, *J. Phys. Chem. Lett.*, 2017, **8**, 489–493.
21 H. Huang, M. I. Bodnarchuk, S. V. Kershaw, M. V. Kovalenko and A. L. Rogach, *ACS Energy Lett.*, 2017, **2**, 2071–2083.
22 X. Zheng, B. Chen, J. Dai, Y. Fang, Y. Bai, Y. Lin, H. Wei, X. C. Zeng and J. Huang, *Nat. Energy*, 2017, **2**, 17102.
23 G. Li, J. Huang, H. Zhu, Y. Li, J.-X. Tang and Y. Jiang, *Chem. Mater.*, 2018, **30**, 6099–6107.
24 L. M. Wheeler, E. M. Sanehira, A. R. Marshall, P. Schulz, M. Suri, N. C. Anderson, J. A. Christians, D. Nordlund, D. Sokaras, T. Kroll, S. P. Harvey, J. J. Berry, L. Y. Lin and J. M. Luther, *J. Am. Chem. Soc.*, 2018, **140**, 10504–10513.
25 H. Wu, Y. Zhang, M. Lu, X. Y. Zhang, C. Sun, T. Q. Zhang, V. L. Colvin and W. W. Yu, *Nanoscale*, 2018, **10**, 4173–4178.
26 T. Chiba and J. Kido, *J. Mater. Chem. C*, 2018, **6**, 11868–11877.
27 H. C. Cao, S. Lin, Z. H. Ma, X. D. Li, J. Li and L. X. Zhao, *IEEE Electron Device Lett.*, 2019, **40**, 267–270.
28 X. Chen, L. C. Peng, K. K. Huang, Z. Shi, R. G. Xie and W. S. Yang, *Nano Res.*, 2016, **9**, 1994–2006.
29 T. Rajh, L. X. Chen, K. Lukas, T. Liu, M. C. Thurnauer and D. M. Tiede, *J. Phys. Chem. B*, 2002, **106**, 10543–10552.
30 J. Zhou, Y. Liu, J. Tang and W. Tang, *Mater. Today*, 2017, **20**, 360–376.
31 Z. Li, L. Kong, S. Huang and L. Li, *Angew. Chem.*, 2017, **129**, 8246–8250.
32 G. Yuan, C. Ritchie, M. Ritter, S. Murphy, D. E. Gómez and P. Mulvaney, *J. Phys. Chem. C*, 2017, **122**, 13407–13415.
33 B. Conings, J. Drijkoningen, N. Gauquelin, A. Babayigit, J. D'Haen, L. D'Olieslaeger, A. Ethirajan, J. Verbeeck, J. Manca, E. Mosconi, F. D. Angelis and H.-G. Boyen, *Adv. Energy Mater.*, 2015, **5**, 1500477.
34 M. H. Garner, R. Hoffmann, S. Rettrup and G. C. Solomon, *ACS Cent. Sci.*, 2018, **4**, 688–700.
35 J. H. Li, L. M. Xu, T. Wang, J. Z. Song, J. W. Chen, J. Xue, Y. H. Dong, B. Cai, Q. S. Shan, B. N. Han and H. B. Zeng, *Adv. Mater.*, 2017, **29**, 1603885.
36 A. Swarnkar, A. R. Marshall, E. M. Sanehira, B. D. Chernomordik, D. T. Moore, J. A. Christians, T. Chakrabarti and J. M. Luther, *Science*, 2016, **354**, 92–95.
37 G. Niu, W. Li, J. Li, X. Liang and L. Wang, *RSC Adv.*, 2017, **7**, 17473–17479.
38 B. A. Koscher, J. K. Swabeck, N. D. Bronstein and A. P. Alivisatos, *J. Am. Chem. Soc.*, 2017, **139**, 6566–6569.
39 Y. Tong, M. Fu, E. Bladt, H. Huang, A. F. Richter, K. Wang, P. Müller-Buschbaum, S. Bals, P. Tamarat, B. Lounis, J. Feldmann and L. Polavarapu, *Angew. Chem., Int. Ed.*, 2018, **57**, 16094–16098.
40 B. J. Bohn, Y. Tong, M. Gramlich, M. L. Lai, M. Döblinger, K. Wang, R. L. Z. Hoye, P. Müller-Buschbaum, S. D. Stranks, A. S. Urban, L. Polavarapu and J. Feldmann, *Nano Lett.*, 2018, **18**, 5231–5238.
41 S. C. Zhu, L. X. Zhao, C. Yang, H. C. Cao, Z. G. Yu and L. Liu, GaN-based flip-chip parallel micro LED array

Open Access Article. Published on 09 July 2019. Downloaded on 7/10/2019 9:06:30 AM.
This article is licensed under a Creative Commons Attribution 3.0 Unported Licence.

for visible light communication, *Proc. SPIE*, 2017, 102441Y.
42 http://www.shinetsusilicone-global.com/products/usage/led/index.shtml.
43 http://www.shinetsusilicone-global.com/catalog/pdf/LED Encapsulant_e.pdf.
44 S. Rajbhandari, J. J. D. McKendry, J. Herrnsdorf, H. Chun, G. Faulkner, H. Haas, I. M. Watson, D. O'Brien and M. D. Dawson, *Semicond. Sci. Technol.*, 2017, **32**, 023001.
45 C. Lee, C. Shen, H. M. Oubei, M. Cantore, B. Janjua, T. K. Ng, R. M. Farrell, M. M. El-Desouki, J. S. Speck and S. Nakamura, *Opt. Express*, 2015, **23**, 29779–29787.
46 I. Dursun, C. Shen, M. R. Parida, J. Pan, S. P. Sarmah, D. Priante, N. Alyami, J. Liu, M. I. Saidaminov and M. S. Alias, *ACS Photonics*, 2016, **3**, 1150–1156.
47 T. R. Chen, W. L. Chen, B. J. Foley, J. Lee, J. P. Ruff, J. P. Ko, C. M. Brown, L. W. Harriger, D. Zhang and C. Park, *Proc. Natl. Acad. Sci. U. S. A.*, 2017, **114**, 7519–7524.
48 O. Yaffe, Y. S. Guo, L. Z. Tan, D. A. Egger, T. Hull, C. C. Stoumpos, F. Zheng, T. F. Heinz, L. Kronik and M. G. Kanatzidis, *Phys. Rev. Lett.*, 2017, **118**, 136001.
49 J. F. Yang, X. M. Wen, H. Z. Xia, R. Sheng, Q. S. Ma, J. Kim, P. Tapping, T. Harada, T. W. Kee and F. Huang, *Nat. Commun.*, 2017, **8**, 14120.

 This journal is © The Royal Society of Chemistry 2019